



## City Research Online

### City, University of London Institutional Repository

---

**Citation:** Mergos, P.E. & Kappos, A. J. (2010). Seismic damage analysis including inelastic shear-flexure interaction. *Bulletin of Earthquake Engineering*, 8(1), pp. 27-46. doi: 10.1007/s10518-009-9161-2

This is the unspecified version of the paper.

This version of the publication may differ from the final published version.

---

**Permanent repository link:** <https://openaccess.city.ac.uk/id/eprint/3526/>

**Link to published version:** <https://doi.org/10.1007/s10518-009-9161-2>

**Copyright:** City Research Online aims to make research outputs of City, University of London available to a wider audience. Copyright and Moral Rights remain with the author(s) and/or copyright holders. URLs from City Research Online may be freely distributed and linked to.

**Reuse:** Copies of full items can be used for personal research or study, educational, or not-for-profit purposes without prior permission or charge. Provided that the authors, title and full bibliographic details are credited, a hyperlink and/or URL is given for the original metadata page and the content is not changed in any way.

---

---

---

City Research Online:

<http://openaccess.city.ac.uk/>

[publications@city.ac.uk](mailto:publications@city.ac.uk)

---

# Seismic damage analysis including inelastic shear-flexure interaction

Panagiotis E. Mergos<sup>1</sup> Andreas J. Kappos<sup>2</sup>

<sup>1</sup> Graduate Student, Lab. of Concrete and Masonry Structures, Department of Civil Engineering, Aristotle University of Thessaloniki, Greece

<sup>2</sup> Professor, Lab. of Concrete and Masonry Structures, Department of Civil Engineering, Aristotle University of Thessaloniki, 54124 Greece

(tel: +30 2310 995743, e-mail: ajkap@civil.auth.gr )

**Abstract** The paper focusses on seismic damage analysis of reinforced concrete (R/C) members, accounting for shear-flexure interaction in the inelastic range. A finite element of the beam-column type for the seismic analysis of R/C structures is first briefly described. The analytical model consists of two distributed flexibility sub-elements which interact throughout the analysis to simulate inelastic flexural and shear response. The finite element accounts for shear strength degradation with inelastic curvature demand, as well as coupling between inelastic flexural and shear deformations after flexural yielding. Based on this model, a seismic damage index is proposed taking into account both inelastic flexural and shear deformations, as well as their interaction. The finite element and the seismic damage index are used to analyse the response of R/C columns tested under cyclic loading and failing either in shear or in flexure. It is shown that the analytical model and damage index can predict and describe well the hysteretic response of R/C columns with different types of failure.

**Keywords** reinforced concrete members; distributed flexibility models; shear-flexure interaction; damage indices

## 1 INTRODUCTION

The vast majority of existing R/C structures has not been designed according to modern seismic codes. These structures are very likely to experience brittle types of shear failure with grave consequences during a major seismic event. Therefore, a complete and reliable seismic assessment of these structures should account for inelastic shear effects.

The first step to perform a realistic seismic damage analysis is to develop an analytical model which is able to predict accurately nonlinear structural behaviour during a seismic event. Explicit modelling of inelastic shear may play a key role in this respect, especially in the case of gravity load designed (GLD) frame structures.

Relatively few researchers have attempted to explicitly include inelastic shear response in assessment of R/C structures (Takayanagi et al. 1979; Thom 1983; D'Ambrisi and Filippou 1997; Ricles et al. 1998; Petrangeli et al. 1999; Pincheira et al. 1999; Lee and Elnashai 2001; Elwood and Moehle 2003; Cosenza et al. 2006; Marini and Spacone 2007). The limited number of such studies, compared to those dealing with predominantly flexural response, should be attributed to the fact that determination of shear strength of R/C members, and especially of shear deformation characteristics, are still controversial issues.

The authors recently developed a new finite element (Mergos and Kappos 2008) belonging to the class of phenomenological, 'member type', models. It consists of two sub-elements with distributed flexibility, representing inelastic flexural and shear response. The two sub-elements are connected by equilibrium and interact throughout the analysis to capture the shear-flexure interaction effect. Following this formulation, the proposed model is able to capture spread of flexural yielding, as well as spread of shear cracking, in R/C members. The model accounts for shear strength degradation with inelastic curvature demand (Priestley et al. 1994), as well as coupling between inelastic flexural and shear deformations after flexural yielding, observed in many experimental studies (Oesterle et al. 1980; Saatcioglu and Ozcebe 1989).

The second step for a complete seismic damage analysis is to quantify numerically the level of structural damage caused by an earthquake. A great number of seismic damage indices have been proposed in the literature (Kappos 1997). The level of sophistication of the existing damage indicators varies from the simple and traditional displacement ductility to cumulative damage models which attempt to take into account damage caused by repeated cycling.

However, a major drawback of existing indices is that they have been formulated and verified almost exclusively on the basis of flexure damage mechanisms and possibly combining shear transfer mechanisms to the above, within the same constitutive law, e.g. moment-rotation (Park et al. 1987).

Williams et al. (1997) evaluated eight existing damage indices by comparison with a series of single-component tests using a variety of moment to shear ratios and stirrup spacings. They found that none of the proposed indices followed a clear shear-dependent trend.

Garstka et al. (1993) have proposed, on the basis of nine test results involving beams with different shear spans, a shear-flexure interaction model, wherein the proposed damage index is expressed as a nonlinear combination of damage due to shear and flexure. Both components of the damage index are based purely on energy absorption, using a concept suggested by Meyer et al. (1988). However, the combined failure criterion of Garstka et al. (1993) has been calibrated with a very limited set of data, while further calibration becomes difficult since experimentally-measured dissipated energies of monotonically and cyclically loaded concrete members up to failure are required for various bending-shear combinations.

Based on the finite element developed by the authors of this study, which is described briefly in the next section, a new seismic damage index considering inelastic shear-flexure interaction effects is presented in this paper. The proposed damage index is applied in the damage analysis of reinforced concrete column specimens failing either in shear or in flexure. It is found that the new damage index describes reliably the behaviour of both types of R/C members up to failure.

## **2 FINITE ELEMENT WITH SHEAR-FLEXURE INTERACTION**

### **2.1 Flexural Sub-element**

The flexural sub-element is used for modelling the bending behaviour of an R/C member subjected to cyclic loading before, as well as after, yielding of the reinforcement. It consists of a set of rules governing the hysteretic moment-curvature ( $M-\phi$ ) behaviour of the member end sections, and a spread plasticity model describing flexural stiffness distribution along the entire member.

The  $M-\phi$  relationship at each end section of the member is described by the primary curve and the rules determining its hysteretic behaviour. The primary  $M-\phi$  relationship is derived using standard flexural analysis of the critical cross-section, with appropriate constitutive laws for concrete and steel. The relationship is then

approximated by a bilinear (elastoplastic with strain hardening) curve. The multi-linear, ‘yield-oriented’ with slip, model of Sivaselvan and Reinhorn (1999) was adopted herein for describing the hysteretic  $M-\phi$  behaviour. The hysteretic model was appropriately modified by the writers to be compatible with a bilinear skeleton curve (Mergos and Kappos 2008).

To capture the variation of the section flexibility along an R/C member, a spread plasticity formulation has to be developed. The flexural sub-element presented herein and shown in Figure 1 is based primarily on the model by Valles et al. (1996). In Figure 1,  $L$  is the length of the member;  $EI_A$  and  $EI_B$  are the current flexural rigidities of the sections at the ends A and B, respectively;  $EI_o$  is the stiffness at the intermediate part of the element and  $\alpha_A$  and  $\alpha_B$  are the ‘yield penetration’ coefficients which specify the proportion of the element where the acting moment is greater than the end section yield moment (Mergos and Kappos 2008).

The flexural spread plasticity model presented in this work differs from the one of Valles et al. (1996) in that constant rigidity is assumed along the yield penetration lengths, and nonlinear moment distribution due to possible gravity load effects is taken into account in calculating the yield penetration coefficients (Fig. 1); the latter feature is particularly important in the case of beam elements.

## **2.2 Shear Sub-element**

The shear sub-element represents the hysteretic shear behaviour of the R/C member prior and subsequent to shear cracking. It consists of a set of rules determining  $V-\gamma$  (shear force vs. shear distortion) hysteretic behaviour of the member end regions, and a shear spread plasticity model defining shear stiffness distribution along the entire member. In this study, shear distortion,  $\gamma$ , is defined as the average shear deformation along the discrete regions (cracked or uncracked) of the shear sub-element.

The  $V-\gamma$  relationship of each member end region is determined by the primary curve and the rules governing its hysteretic behaviour. Initially, the backbone curve is calculated without including shear-flexure interaction effects (initial backbone). Then, shear flexure interaction effects are modelled by assigning an appropriate analytical procedure.

The  $V$ - $\gamma$  initial primary curve consists of three branches (Fig. 2), but only two different slopes, as explained later on. The first branch connects the origin and the shear cracking point, which is defined as the point where the nominal principal tensile stress exceeds the mean tensile strength of concrete. The shear cracking point is determined following a procedure proposed by Sezen and Moehle (2004) and assuming constant shear stiffness in this range of the response.

The second and third branches of the initial primary curve have the same slope and connect the shear cracking point to the point corresponding to the onset of yielding of transverse reinforcement ( $V_{uo}$ ,  $\gamma_u$ ). The latter is taken as the ‘failure’ point in this study (Mergos and Kappos 2008). The second and third branches are separated at the point corresponding to flexural yielding ( $V_y$ ,  $\gamma_y$ ). This approach was adopted in order to distinguish hysteretic shear behaviour before and after flexural yielding (Ozcebe and Saatcioglu 1989).

The mean shear distortion at the onset of transverse reinforcement yielding,  $\gamma_u$ , is estimated using the truss analogy approach proposed by Park and Paulay (1975) and Kowalsky and Priestley (1995). According to this approach, in a cracked member the shear deformation will arise from the extension of transverse reinforcement and the compression of the diagonal compression struts.

Regression analyses by the writers (Mergos and Kappos 2008) showed that best correlation with experimental results was achieved when, in calculating  $\gamma_u$  from the truss analogy approach, the angle  $\theta$  was taken equal to  $35^\circ$  (unless limited to larger angles by the potential corner-to-corner crack) and the derived value was then multiplied by two modification factors. The first modification factor,  $\kappa$ , takes into account the influence of the axial load and the second modification factor,  $\lambda$ , represents the influence of the column aspect ratio. Regarding shear strength,  $V_u$ , the approach proposed by Priestley et al. (1994) is invoked, which has been developed for both circular and rectangular columns. According to this approach, the concrete contribution to maximum shear strength is a function of a parameter  $k$  which decreases with maximum curvature ductility demand developed in the critical cross section. For the initial shear primary curve,  $V_{uo}$  is derived by setting the value of  $k$  corresponding to curvature ductility demand  $\mu_{\phi} \leq 3$  (i.e. no strength degradation). In the finite element of this study, shear strength degrades based on maximum curvature ductility demand. This is achieved by using the procedure described in the following.

First, at each time step  $i$  of the analysis, maximum curvature ductility demand of the critical cross section  $j$  ( $j=A,B$ ),  $\mu_{\phi j, \max}^i$ , of the flexural sub-element is defined. Then, the corresponding  $k_j^i$  factor is determined (Priestley et al. 1994) and this factor is used to calculate current shear strength,  $V_{u,j}^i$ ; hence the shear strength degradation is

$$DV_{u,j}^i = V_{uo,j}^i - V_{u,j}^i \quad (1)$$

This shear strength degradation is then modelled by reducing the ordinate of the backbone curve of the respective end-section of the shear sub-element, as shown schematically in Fig. 3.

In order to re-establish equilibrium, the shear force increment at the next time step  $i+1$ ,  $\Delta V_j^{i+1}$ , is calculated by the total moment distribution at this time step minus the respective shear force of the previous time step,  $V_j^i$ . Assuming uniform gravity load distribution, the following equations are obtained

$$\Delta V_A^{i+1} = -\frac{q \cdot L}{2} + \frac{(M_A^{i+1} - M_B^{i+1})}{L} - V_A^i \quad (2)$$

$$\Delta V_B^{i+1} = \frac{q \cdot L}{2} + \frac{(M_A^{i+1} - M_B^{i+1})}{L} - V_B^i \quad (3)$$

Assuming that the end section of the shear sub-element still remains at the loading phase, the shear force increments calculated by Eqs (2)-(3) give rise to the respective shear strain increments,  $\Delta \gamma_j^{i+1}$ , defined by Eq. (4) and shown schematically in Fig 3.

$$\Delta \gamma_j^{i+1} = \frac{\Delta V_j^{i+1}}{GA_1} \quad (4)$$

Combining the analytical procedure shown in Fig. 3 and the relationship between curvature ductility demand and strength of concrete shear-resisting mechanisms proposed in Priestley et al. (1994), yields the modified shear primary curve shown in Fig. 4; in this figure hardening of the flexural primary curve has been exaggerated for illustration purposes. Furthermore, it is assumed that curvature ductility capacity of the critical cross section exceeds the value of 15 (which is often not the case in old-type members) and that the element fails in shear *after* yielding in flexure.

As can be seen in Fig. 4, by adopting the analytical procedure described above, coupling between inelastic flexural and shear displacements is also achieved. More particularly, it is observed that shear displacements increase more rapidly when curvature ductility demand exceeds the value of 3. This increase is sharper for  $3 < \mu_\phi \leq 7$  and becomes smoother for  $7 < \mu_\phi \leq 15$ . Finally, for  $\mu_\phi > 15$ , shear displacements tend to increase at the same rate as they do for  $\mu_\phi \leq 3$ . In all cases, by using this analytical procedure, shear deformation at shear failure will be equal to  $\gamma_u$ . These observations are in accordance with the truss analogy approach (Park and Paulay 1975; Kowalsky and Priestley 1995) as explained in Mergos and Kappos (2008).

Hysteretic shear behaviour ( $V$ - $\gamma$ ) was modelled using the proposals by Ozcebe and Saatcioglu (1989) as a basis, with several modifications and improvements. Although this hysteretic model has been calibrated against experimental results and was found to yield a reasonable match, it has not been designed with a view to being incorporated in a dynamic nonlinear analysis framework. The authors proposed appropriate modifications regarding the hysteretic rules of the unloading and reloading branches of the specific model which can be found in Mergos and Kappos (2008).

To capture variation of shear stiffness along a concrete member, the authors proposed a shear spread-plasticity model formulation. In this model, shear rigidity distribution along a concrete member is assumed to have the form shown in Fig. 5, where  $GA_A$  and  $GA_B$  are the current shear rigidities of the regions at the ends A and B, respectively;  $GA_o$  is the shear stiffness at the intermediate part of the element;  $\alpha_{As}$  and  $\alpha_{Bs}$  are the shear cracking penetration coefficients, which specify the proportion of the element where the acting shear is greater than the shear cracking force of the end section. Analytical information on the calculation of the shear cracking penetration coefficients, as well as the coefficients of the flexibility matrix of the shear sub-element can be found in Mergos and Kappos (2008).

### **3 SEISMIC DAMAGE INDEX**

By definition, a seismic damage index is a quantity with zero value when no damage occurs and of value of 1 (100%) when failure or collapse occurs (Kappos

1997). However, an R/C member may fail either in flexure or in shear. Hence, an appropriate local seismic damage index,  $D_{tot}$ , for such a member should become equal to unity when the respective end of the member reaches its flexure *or* shear deformation capacity. A general mathematical relationship that satisfies the aforementioned limitations is

$$D_{tot} = 1 - (1 - D_{fl})^{\alpha} \cdot (1 - D_{sh})^{\gamma} \quad (5)$$

where  $D_{tot}$  is the total local damage index of the concrete member ( $0 \leq D_{tot} \leq 1$ ) representing total damage of the member;  $D_{fl}$  is the flexural damage index ( $0 \leq D_{fl} \leq 1$ ), representing flexural damage of the member;  $D_{sh}$  is the shear damage index ( $0 \leq D_{sh} \leq 1$ ) representing shear damage of the member;  $\alpha$  is an exponent related to the importance of the flexural damage index  $D_{fl}$  to the total damage index  $D_{tot}$ , and  $\gamma$  is an exponent related to the importance of the shear damage index  $D_{sh}$  to the total damage index  $D_{tot}$ .

In Equation (5), when no flexural or shear damage in the concrete element has occurred ( $D_{fl}=D_{sh}=0$ ) the total damage index  $D_{tot}$  remains equal to zero. However, if flexural failure occurs ( $D_{fl}=1$ ) then  $D_{tot}$  becomes equal to unity independently from the value of the respective shear damage index,  $D_{sh}$ . In a similar fashion, when shear failure occurs ( $D_{sh}=1$ ),  $D_{tot}$  becomes equal to unity irrespectively from the condition of the member in terms of flexural behaviour.

Calculation of  $D_{tot}$ , as given by Equation (5), may be strongly influenced by the values adopted in the analysis for the exponents  $\alpha$  and  $\gamma$ . However, by assigning physically meaningful observations regarding structural damage in R/C elements, these values can be uniquely defined, as described in the following.

Total damage in an R/C member can be considered as a combination of damage due to inelastic flexural effect and inelastic shear effect. Consequently, the total damage index  $D_{tot}$  should obtain greater values than the respective flexural and shear damage indices; nevertheless  $D_{tot}$  should not exceed 1 (that corresponds to member failure). Equation (5) satisfies the aforementioned limitation only when  $\alpha$  and  $\gamma$  assume values greater than 1.

Moreover, it is physically meaningful to assume that when one type of damage (flexure or shear) is negligible in the R/C member, the total damage in the member is due to the other mechanism (shear or flexure); i.e. if  $D_{fl}=0$ , it is rational to

assume that  $D_{tot}=D_{sh}$ , and vice versa. In equation (5) this can be achieved only when  $\alpha=\gamma=1$ .

Based on all the above considerations, Equation (6) is finally proposed herein for determining  $D_{tot}$  from  $D_{fl}$  and  $D_{sh}$ :

$$D_{tot} = 1 - (1 - D_{fl}) \cdot (1 - D_{sh}) \quad (6)$$

Figure 6 illustrates variation of  $D_{tot}$  for all the possible combinations of  $D_{fl}$  and  $D_{sh}$ . It can be seen that  $D_{tot}$  takes a zero value only when both  $D_{fl}$  and  $D_{sh}$  are equal to zero (no damage in flexure or in shear). Furthermore, it is obvious that when one of the damage indices ( $D_{fl}$ ,  $D_{sh}$ ) becomes equal to one (flexural or shear failure respectively) then  $D_{tot}$  becomes equal to one as well, irrespectively from the value of the other index. The physical meaning of this observation is that the R/C member has reached its lateral force capacity when either flexural or shear failure occurs.

Fig. 7 presents variation of  $D_{tot}$  with  $D_{max}$  for the two edge values of  $D_{min}$  where  $D_{max}$  and  $D_{min}$  are the maximum and minimum values, respectively, of  $D_{fl}$  or  $D_{sh}$ . It is obvious that when  $D_{min}=0$ , then  $D_{tot}=D_{tot,min}=D_{max}$ , meaning that when one type of damage is negligible then the total damage of the member can be assumed equal to the other type of structural damage. When  $D_{min}=D_{max}$ ,  $D_{tot}$  obtains its maximum values,  $D_{tot,max}$  which can be significantly higher than  $D_{max}$ , as can be observed in Fig. 7. For all the intermediate values of  $D_{min}$  ( $0 < D_{min} < D_{max}$ ),  $D_{tot}$  lies always between the continuous and dotted line of the same figure ( $D_{tot,max}$  and  $D_{tot,min}$  respectively) which can be considered as the upper and lower limit, respectively, of  $D_{tot}$  as a function of  $D_{max}$ . In all cases,  $D_{tot}$  is equal or greater than  $D_{max}$ .

In all damage assessment procedures, for the calculation of the total damage index  $D_{tot}$ , determination of the individual damage indices  $D_{fl}$  and  $D_{sh}$  is first required. In general, damage in R/C elements is related to irrecoverable (inelastic) deformation. Therefore, any damage variable should preferably refer to a certain deformation quantity (Kappos 1997).

By definition, the flexural damage index  $D_{fl}$  should refer to a local, purely flexural, deformation variable. The best choice for this case is the curvature  $\phi$  developed at the respective end of the R/C member. Similarly, the shear damage index  $D_{sh}$  should refer to the shear distortion  $\gamma$  developed at the respective end

region of the member, as defined also in the shear sub-element described in Section 2.2.

Following the basic definition of a seismic damage index,  $D_{fl}$  and  $D_{sh}$  must have a zero value when no flexural or shear damage takes place in the R/C member and they must become equal to unity when flexural or shear failure respectively occurs.

Flexural damage in an R/C member occurs when the maximum developed curvature  $\varphi_{max}$  at the respective end of the member exceeds a threshold value  $\varphi_o$ , below which virtually elastic behaviour occurs, in the sense that no permanent deformation is visible and therefore no damage is detected. In an analogous fashion, shear damage in an R/C member takes place when maximum shear distortion  $\gamma_{max}$  becomes greater than the respective threshold value in shear,  $\gamma_o$ .

Flexural failure develops in an R/C member when the maximum developed curvature  $\varphi_{max}$  at the respective end of the member reaches available curvature capacity  $\varphi_u$ . Curvature capacity  $\varphi_u$  can be considered as the minimum value from those corresponding to hoop fracture due to a strain arising from the expansion of the concrete core (Priestley et al. 1996), fracture of the longitudinal reinforcement in the tension zone, and buckling of the compression bars (Papia and Russo 1989). Shear failure occurs when the maximum shear distortion  $\gamma_{max}$  at the end region of the R/C member reaches or exceeds the respective available shear distortion capacity  $\gamma_u$ . As explained in Section 2.2, it is assumed in this study that  $\gamma_u$  coincides with the onset of yielding of transverse reinforcement. In general, this is a conservative approach; nevertheless, it is very realistic in the case of R/C members with non-ductile transverse reinforcement detailing which happen to be the members most amenable to shear types of failure.

Two general relationships for the flexural and shear damage index, satisfying the aforementioned limitations, are the ones given in Equations (7) and (8).

$$D_{fl} = 1 - \left( 1 - \frac{\varphi_{max} - \varphi_o}{\varphi_u - \varphi_o} \right)^\xi \quad (7)$$

$$D_{sh} = 1 - \left( 1 - \frac{\gamma_{max} - \gamma_o}{\gamma_u - \gamma_o} \right)^\rho \quad (8)$$

It is obvious that in Equations (7) and (8) when  $\varphi_{max} < \varphi_o$  or  $\gamma_{max} < \gamma_o$  then  $\varphi_{max} = \varphi_o$  and  $\gamma_{max} = \gamma_o$  respectively should be assumed to avoid negative values for  $D_{sh}$  and  $D_{tot}$ .

In the same equations,  $\xi$  and  $\rho$  are exponents determining the rate at which flexural or shear damage increases with the normalized ratios  $(\varphi_{\max}-\varphi_o)/(\varphi_u-\varphi_o)$  and  $(\gamma_{\max}-\gamma_o)/(\gamma_u-\gamma_o)$  respectively. It is worth pointing out, that these normalized ratios represent special cases of Equations (7) and (8) by setting  $\xi=\rho=1$ .

Clearly, exponents  $\xi$  and  $\rho$  should be determined on the basis of available experimental data. However, until today, only limited calibration of the damage indices has been performed against observed damage in laboratory tests or post-earthquake investigations. Since experimental data are either unavailable or inconclusive, it seems better to assign values to  $\xi$  and  $\rho$  that would provide the most reasonable values to the total damage index  $D_{\text{tot}}$  for the whole range of the possible combinations of the aforementioned normalized deformation ratios. By combining Equations (6), (7) and (8), the following equation arises for the total damage index,  $D_{\text{tot}}$ :

$$D_{\text{tot}} = 1 - \left( 1 - \frac{\varphi_{\max} - \varphi_o}{\varphi_u - \varphi_o} \right)^{\xi} \cdot \left( 1 - \frac{\gamma_{\max} - \gamma_o}{\gamma_u - \gamma_o} \right)^{\rho} \quad (9)$$

Until today, there exist no sufficient and reliable data on the relative importance of the flexural and shear deformations to the total damage of a concrete member; in fact, this relative importance is very difficult to quantify. It is worth noting in this respect that the issue here is not whether shear failure is more brittle than flexural one, but whether the amount of damage inflicted by either type of inelastic deformation (flexural or shear) is different when the value of the corresponding normalized deformation ratios of Equation (9) is the same. Therefore, it appears more logical, at least at this stage of research, to assume equal importance of the flexural normalized deformation ratio and the shear deformation ratio to the total damage index,  $D_{\text{tot}}$ . Hence, it is assumed in this study that  $\xi=\rho$ .

By assigning the following definitions:

$$r_{\max} = \max \left[ \frac{\varphi_{\max} - \varphi_o}{\varphi_u - \varphi_o}, \frac{\gamma_{\max} - \gamma_o}{\gamma_u - \gamma_o} \right] \quad (10)$$

$$r_{\min} = \min \left[ \frac{\varphi_{\max} - \varphi_o}{\varphi_u - \varphi_o}, \frac{\gamma_{\max} - \gamma_o}{\gamma_u - \gamma_o} \right] \quad (11)$$

Equation (9) can now be written as

$$D_{tot} = 1 - (1 - r_{max})^{\xi} \cdot (1 - r_{min})^{\xi} \quad (12)$$

It can be inferred by Equation (12) that  $D_{tot}$  assumes minimum values,  $D_{tot,min}$ , as a function of  $r_{max}$  when it is  $r_{min}=0$  and that  $D_{tot}$  reaches maximum values,  $D_{tot,max}$ , as a function of  $r_{max}$  when  $r_{min}$  becomes equal to  $r_{max}$ . For all the other values of  $r_{min}$  ( $0 < r_{min} < r_{max}$ ),  $D_{tot}$  remains between  $D_{tot,min}$  and  $D_{tot,max}$ .

Fig. 8 illustrates variation of  $D_{tot,min}$  with  $r_{max}$  for four discrete values of  $\xi$ . It can be seen, that for  $\xi=1/3$ ,  $D_{tot}$  increases from a value of 0.63 to 1.0 as  $r_{max}$  increases from 0.95 to 1.0. This abrupt increase in  $D_{tot}$  is contrary to both experimental evidence of damage and to engineering judgment. Thus,  $\xi=1/3$  is not a proper value for determining  $D_{tot}$ . For the other values of  $\xi$  in Fig. 8,  $D_{tot,min}$  varies in a relatively smooth way as a function of  $r_{max}$ .

Fig. 9 illustrates variation of  $D_{tot,max}$  with  $r_{max}$  for the same four discrete values of  $\xi$ . It can be seen, that for  $\xi=4/3$ ,  $D_{tot}$  has become equal to 0.90 for  $r_{max}=0.60$  meaning that as  $r_{max}$  increases from 0.6 to 1 the additional damage is almost negligible. This also conflicts with available experimental evidence. The same occurs for  $\xi=1$ , in which case  $D_{tot}$  becomes equal to 0.88 for  $r_{max}=0.65$ .

On the basis of the above, the solution deemed to provide reasonable values to both  $D_{tot,min}$  and  $D_{tot,max}$  is  $\xi=2/3$ . In figure 10, variation of both  $D_{tot,min}$  and  $D_{tot,max}$  with  $r_{max}$  for  $\xi=2/3$  is illustrated. It can be seen that  $D_{tot,min}$  and  $D_{tot,max}$  curves are almost symmetric with respect to the 45degrees line. It is clear from this figure, that this solution assures in all cases smooth variation of  $D_{tot}$  with  $r_{max}$  permitting a clear differentiation of the various levels of damage. In all cases the values of  $D_{tot}$  lie between the  $D_{tot,min}$  and  $D_{tot,max}$  curves. For example, for  $r_{max}=0.5$ ,  $D_{tot}$  varies from 0.37 ( $r_{min}=0$ ) to 0.62 ( $r_{min}=r_{max}=0.5$ ) which represents a 67% increase to the value of the total damage index. In order to obtain such an increase for the case of  $r_{min}=0$ ,  $r_{max}$  must rise up to 0.77 representing a 54% increase in the respective value of  $r_{max}$ . The above show that the proposed formulation of the total damage index  $D_{tot}$  can represent the combined damage due to the simultaneous inelastic flexural and shear effect in R/C members.

Another critical issue regarding the determination of  $D_{tot}$  is the actual definition of the threshold values  $\phi_o$  and  $\gamma_o$  below which no damage is detected. Values corresponding to flexural and shear cracking or flexural and shear yielding may be adopted. However, due to the nonlinear, inelastic behaviour of R/C from the very early stages of response, definition of  $\phi_o$  and  $\gamma_o$  is not always straightforward.

Furthermore, for a broad class of R/C members, the aforementioned values represent only a very small fraction of  $\varphi_u$  and  $\gamma_u$  respectively; hence, their inclusion in the determination of  $D_{tot}$  has only a minor influence on the results (see section 4). In this study, for simplification reasons, it is assumed that  $\varphi_o=\gamma_o=0$ .

On the basis of the aforementioned observations, Equation (13) is invoked in this study for the calculation of  $D_{tot}$ .

$$D_{tot} = 1 - \left(1 - \frac{\varphi_{max}}{\varphi_u}\right)^{2/3} \cdot \left(1 - \frac{\gamma_{max}}{\gamma_u}\right)^{2/3} \quad (13)$$

Based on this equation, Fig. 11 illustrates variation of  $D_{tot}$  for all pairs of the normalized ratios  $\varphi_{max}/\varphi_u$  and  $\gamma_{max}/\gamma_u$ . In this figure, it can be seen that  $D_{tot}$  takes a zero value only when both maximum curvature and shear distortion demand have also zero values. Furthermore, when the R/C member reaches its deformation capacity in flexure ( $\varphi_{max}=\varphi_u$ ),  $D_{tot}$  becomes equal to unity regardless of the member state in shear; similarly for the case where maximum shear distortion demand  $\gamma_{max}$  reaches  $\gamma_u$ . In both cases, the R/C member starts to lose its lateral force capacity and can be considered as ‘failed’ following a more or less conservative approach.

It is important to note that Equation (13) can be incorporated only in a finite element, like the one described earlier in this study, which utilizes moment-curvature and shear force – shear strain hysteretic relationships at the two ends of the member for the calculation of the element flexibility matrix. It cannot be applied for example to finite elements where all types of inelastic deformations along the member are lumped to zero length rotational springs at the member ends. Furthermore, it must be stated, that this equation may lead to erroneous results if it is applied in the nonlinear analyses of R/C structures where increase of shear deformations after flexural yielding (shear-flexure interaction) is disregarded, as it will be shown in the correlation examples of this study.

A limitation of the proposed equation for  $D_{tot}$  is the fact that it does not account for cumulative damage effects due to repeated cycling. Kappos and Xenos (1996) assessed the importance of the energy term in the combined damage index of Park et al. (1987) considering realistic structures and hysteretic characteristics, realistic seismic inputs, and also a sufficiently rigorous dynamic inelastic analysis procedure. It was found that the contribution of the energy term to the value of the damage index was very low for the case of well-detailed R/C members. However,

for R/C members with poor detailing available data remain ambiguous since calibration against experimental evidence is still very limited. Further consideration should be given to the issue of whether cumulative damage effects should be considered in the case of non-ductile R/C elements.

## **4 CORRELATION WITH EXPERIMENTAL RESULTS**

The proposed member-type finite element model was implemented in a computer program (IDARC/2D) for the nonlinear dynamic analysis of 2D R/C structures (Valles et al. 1996). Bond-slip effects in this study were taken into account indirectly as described in Mergos and Kappos (2008). To validate the model, the program was used to simulate the hysteretic response of several R/C members tested under cyclic loading; results for a flexure-critical member, a member failed in shear after flexural yielding, and a shear-critical member, are presented herein.

Based on the analysis results, the proposed seismic damage index was implemented to describe inelastic damage behaviour of the specific R/C members. Participation of the individual damage mechanisms (flexure and shear), as well as their interaction to the total damage of the R/C elements were investigated. Finally, the proposed index was compared with a well-documented seismic damage index (Park et al. 1987) in order to investigate its capacity in describing evolution of damage in R/C members. The basic findings for each individual R/C column element are presented in the following.

### **4.1 Flexure-critical R/C member**

Lehman and Moehle (1998) tested five circular R/C bridge columns, typical of modern construction, under uniaxial displacement-controlled lateral load reversals. Herein, the specimen designated as 415 is examined; detailed information regarding the experimental variables of the specimen can be found in Mergos and Kappos (2008). This specimen was dominated by flexure, exhibiting stable hysteretic behaviour until failure.

Fig. 12(a) shows the experimental and analytical lateral load vs. total displacement relationship of the specimen. It is seen that the proposed analytical

model predicts well the experimental behaviour up to maximum response.

Fig. 12(b) presents the evolution of the structural damage index  $D_{tot}$  with the experimental load step. Contributions of the flexural and shear inelastic mechanisms are also included. It can be observed that the flexural damage index  $D_{fl}$  prior to flexural yielding, which occurs at step 540, assumes very small values (less than 5%). However, after flexural yielding,  $D_{fl}$  gradually increases up to 87% a value very close to 100% that corresponds to complete failure of the element. Similarly, prior to shear cracking, which takes place at loading step 370,  $D_{sh}$  takes values smaller than 1%. After shear cracking,  $D_{sh}$  increases more rapidly but its final value remains relative small (37%) emphasizing the fact that shear is not critical for this element. It is worth noting that  $D_{sh}$  continues to increase after flexural yielding as a result of the shear-flexure interaction procedure adopted by the finite element of this study.

For the entire range of response,  $D_{tot}$ , due to its formulation, envelopes the two component damage indices. It can be inferred from the figure that immediately after shear cracking,  $D_{tot}$  is governed by  $D_{sh}$ . However, after flexural yielding,  $D_{fl}$  gradually obtains the vital role in the determination of  $D_{tot}$  and at the end of the analysis these two damage indices almost coincide. The final value of  $D_{tot}$  is 92%, which is very close to failure. The small differentiation may be attributed to the fact that the specific R/C member, as can be inferred from Fig. 12(a), fails finally due to repeated cycling at maximum displacement. It is recalled that the proposed damage, in its current formulation, cannot take into account cumulative damage effects.

Fig. 12(c) compares the values of the total and shear damage index when increase of inelastic shear deformations after flexural yielding is taken into account in the finite element model (D1) and when this phenomenon is totally ignored in the analysis (D2). It can be seen that considering inelastic shear-flexure interaction effect leads to an increase of  $D_{sh}$  from 12% to 37% at the end of the analysis. Hence, modelling this effect is a crucial issue in a seismic damage analysis considering inelastic shear mechanisms. The respective differentiation in the values of  $D_{tot}$  is more important during the intermediate steps of the response where  $D_{sh}$  is still significant for the total damage of the member. Nevertheless, at the final stages of the response,  $D1_{tot}$  and  $D2_{tot}$  are almost identical due to the fact

that their values are governed by the flexural damage index.

Finally, in Fig. 12(d) the proposed total damage index is compared with the Park-Ang damage index, which has the general form (Park et al. 1987):

$$D = \frac{\theta_{\max}}{\theta_u} + \beta \cdot \frac{\int M d\theta}{M_y \cdot \theta_u} \quad (14)$$

where the first term is the ratio of maximum recorded rotation to the rotational capacity of the member under monotonic loading conditions and the integral term is the energy dissipation normalized by the product of the yield moment and rotational capacity and scaled by an empirical factor,  $\beta$  determined on the basis of a large number of test results. For this example, the typical value of  $\beta=0.05$  was used as proposed for well-detailed R/C members. Rotational capacity  $\theta_u$  was calculated by using the equivalent plastic hinge length approach with the formula proposed by Priestley et al. (1996).

It can be observed in Fig. 12(d) that the two indices show similar trends and almost identical values at maximum response. This means that both of them are able to describe evolution of structural damage for this flexure-dominated R/C member, however the Park-Ang index provides no indication as to which mechanism is the prevalent one with respect to failure. It is also worth reporting that the Park-Ang damage index failed to predict failure due to repeated cycling of the loading. This fact could be attributed to underestimation of the empirical  $\beta$  factor or overestimation of  $\theta_u$  following the aforementioned semi-empirical procedure, or a combination of both.

## 4.2 Flexure-shear critical R/C member

Lynn et al. (1996) tested 8 full-scale columns, representative of old type construction, having widely-spaced perimeter hoops with 90 degree bends, with or without intermediate hoops, and longitudinal reinforcement with or without lap splices. Herein, the specimen designated as 2CLH18 is examined; experimental variables can be found in Mergos and Kappos (2008).

Fig. 13(a) shows the experimental and analytical lateral load vs. total displacement relationship for the aforementioned specimen. It can be seen that the analytical model is able to represent very well the experimental results. The

specific R/C member exhibited a rather complex behaviour, yielding in flexure and then failing in shear due to drop of its shear capacity caused by shear-flexure interaction. It is important to note that the analytical model was able to capture this response and predict the shear failure of the member at a displacement of 38mm.

Fig. 13(b) shows the evolution of structural damage indices  $D_{fl}$ ,  $D_{sh}$  and  $D_{tot}$  with the experimental load step. It can be observed that the flexural damage index  $D_{fl}$  prior to flexural yielding, which occurs at step 165, obtains very small values (less than 8%). After flexural yielding,  $D_{fl}$  gradually increases up to 79% which means that flexural damage is pretty important for this member. Nevertheless, it is clear that no flexural failure is predicted. Prior to shear cracking, occurring at loading step 150,  $D_{sh}$  takes values smaller than 3%. After shear cracking,  $D_{sh}$  increases sharply and finally becomes equal to unity in accordance with the analytical finite element model which predicted shear failure at the final stage of the response. The total damage index is able of describing the entire history of damage evolution in this column specimen. It can be seen that a first sharp increase of  $D_{tot}$  takes place after shear cracking and another one shortly after, due to flexural yielding. Afterwards,  $D_{tot}$  is influenced similarly by the two component damage indices but at the final steps of the analysis  $D_{tot}$  becomes equal to  $D_{sh}$  emphasizing the fact that, since shear failure occurred, the member as a whole has reached its lateral force capacity.

Fig. 13(c) compares the values of the total and shear damage index when increase of inelastic shear deformations after flexural yielding is taken into account in the finite element model (D1) and when this phenomenon is totally ignored in the analysis (D2). It can be seen that neglecting inelastic shear-flexure interaction effects, results in a value of  $D_{sh}=22\%$  leading to a totally erroneous picture for the shear damage behaviour of the specific column element. The respective value of  $D_{tot}$  is 84% since now the total damage index is governed by  $D_{flex}$ . Obviously, no failure of the R/C member is predicted.

Finally, in Fig. 13(d) the proposed total damage index is compared with the Park-Ang seismic damage index. A value of  $\beta=0.25$  was assumed based on the respective literature for poorly detailed R/C members. It can be observed that although the Park-Ang index assumes high values at the last steps of the response (84%), it is not able to predict failure of this member. This is clearly because of the fact that no separate treatment of shear is made in this damage index.

### 4.3 Shear-critical R/C member

Aboutaha et al. (1999) tested eleven large-scale columns to examine the effectiveness of various types of steel jackets for improving the strength and ductility of columns with inadequate shear resistance. The shear span ratio of the columns was equal to 1.33. All columns were tested without axial load. Three columns were tested as basic unretrofitted specimens. Herein, the unretrofitted specimen designated as SC9 is examined; experimental variables can be found in Mergos and Kappos (2008). The specific squat R/C member was almost totally dominated by shear, experiencing a brittle type of shear failure prior to flexural yielding (Aboutaha et al. 1999).

Fig. 14(a) shows the experimental and analytical lateral load vs. total displacement relationship of the aforementioned specimen. It can be seen that the analytical model is able to capture adequately the pre-peak experimental response.

Overestimation of the initial stiffness may be attributed to the fact that rotations due to inelastic bond-slip effects are not taken into account in this version of the model and to possible overestimation of the shear stiffness prior to shear cracking, which is assumed to be equal to the uncracked (GA) shear stiffness in this study. It is very encouraging that the analytical model was able to predict accurately the displacement at which shear strength starts to degrade rapidly. This was achieved by the correct prediction of  $\gamma_u$  using the modification factors  $\kappa$  and  $\lambda$  (Mergos and Kappos 2008).

Fig. 14(b) shows a comparison of the analytical prediction and the experimental behaviour when shear is not modelled explicitly. It is clear from this figure that ignoring inelastic shear behaviour may lead to totally erroneous results regarding both strength and deformation.

Fig. 14(c) presents the evolution of damage indices  $D_{fl}$ ,  $D_{sh}$  and  $D_{tot}$  with the experimental load step. It is obvious that  $D_{fl}$  is characterized by very small values (less than 12%) over the whole range of response. This is due to the fact that no flexural yielding occurs during the analysis. On the other hand,  $D_{sh}$ , subsequent to shear cracking occurring at load step 35, increases steadily up to unity at the load step where shear failure was predicted by the analysis.  $D_{tot}$  is almost totally dominated by  $D_{sh}$  and the two damage indices become equal at the time of shear

failure. It is worth noting that inelastic shear-flexure interaction was not an issue for this specimen since no flexural yielding occurred during the experimental process.

Finally, Fig. 14(d) illustrates a comparison of the proposed total damage index  $D_{tot}$  and the Park-Ang damage index. It can be seen that the Park-Ang damage index largely underestimates structural damage of this R/C member providing a value of 48% at the time of shear failure. This result clearly shows its weakness to take into consideration inelastic shear effects reliably in a seismic damage analysis. Nevertheless, its final value is significantly greater than the respective value of the flexural damage index,  $D_{fl}$  (calculated using the proposed model). This can be attributed to the fact that the total maximum rotation of the member,  $\theta_{max}$ , is significantly increased by the influence of inelastic shear effects (see Eq. 14) and also to the fact that cumulative damage effects are taken into account by this index.

## 5 CONCLUSIONS

A distributed shear and flexural flexibility model with shear-flexure interaction for seismic assessment of R/C structures has been developed. The model is able of capturing shear strength degradation as well as increase of inelastic shear deformations subsequent to flexural yielding. Based on this finite element model a combined damage index is proposed for the seismic damage analysis of R/C structures. This damage index accounts for both inelastic flexural and shear deformations as well as their interaction.

The proposed finite element and seismic damage index were implemented into the nonlinear static and dynamic analysis program IDARC/2D. They were then used to simulate and describe the nonlinear response of flexure-critical, flexure-shear critical, and shear-critical R/C columns subjected to cyclic lateral loads.

Good agreement between the finite element model and the experimental results was generally observed. Based on these results, the proposed total damage index was found to be able to describe accurately in qualitative, as well as quantitative, terms the evolution of structural damage in R/C members failing either in shear or in flexure.

The simplicity and computational efficiency of the proposed finite element model and seismic damage index, as well as their ability to reasonably capture the behaviour of actual R/C members with different failure modes, make them a valuable tool for the seismic assessment of R/C structures, especially those with non-conforming detailing.

## REFERENCES

- Aboutaha R, Engelhardt D, Jirsa J, Kreger E (1999) Rehabilitation of shear critical concrete columns by use of rectangular steel jackets. *ACI Struct. J.* 96 (1): 68-77
- Cosenza E, Manfredi G, Verderame GA (2006) Fibre model for pushover analysis of underdesigned R/C frames. *Computers and Structures* 84: 904-916
- D'Ambrisi A, Filippou FC (1997) Correlation studies on an R/C frame shaking-table specimen. *Earthquake Engineering & Structural Dynamics* 26: 1021-1040
- Elwood K, Moehle JP (2003) Shake table tests and analytical studies on the gravity load collapse of R/C frames. PEER Report No. 2003/01, Univ. of California, Berkeley
- Garstka B, Krätzig W, Stangenberg F (1993) Damage assessment in cyclically loaded reinforced concrete members. *Proc. Eurodyn 1*: 121-128
- Kappos AJ (1997) Seismic damage indices for R/C buildings. *Progress in Structural Engineering and Materials.* 1(1): 78-87
- Kappos AJ, Xenos A (1996) A reassessment of ductility and energy-based seismic damage indices for reinforced concrete structures. *Proc. Eurodyn 2*: 965-970
- Kowalsky MJ, Priestley MJN (1995) Shear behaviour of lightweight concrete columns under seismic conditions. Report No. SSRP-95/10, University of San Diego, California
- Lee DH, Elnashai AS (2001) Seismic analysis of R/C bridge columns with flexure-shear interaction. *J. of Struct. Eng.* 127(5): 546-553
- Lehman D, Moehle JP (1998) Seismic performance of well confined concrete bridge columns. PEER Report 1998/01, Univ. of California, Berkeley
- Lynn A, Moehle JP, Mahin S, Holmes W (1996) Seismic evaluation of existing reinforced concrete building columns. *Earthquake Spectra* 12(4): 715-739
- Marini A, Spacone E (2006) Analysis of reinforced concrete elements including shear effects. *ACI Struct. J.* 103(5): 645-655
- Mergos PE, Kappos AJ (2008) A distributed shear and flexural flexibility model with shear-flexure interaction for R/C members subjected to seismic loading. *Earthquake Engineering & Structural Dynamics*, published on-line Apr. 4, 2008.
- Meyer I, Krätzig W, Stangenberg F (1988) Damage prediction in reinforced concrete frames under seismic actions. *European Earthquake Engineering* 3(1): 9-15
- Oosterle RG, Fiorato AE, Aristizabal-Ochoa JD, Corley WG (1980) Hysteretic response of reinforced concrete structural walls. *Proc. ACISP-63: Reinforced Concrete Structures subjected to Wind and Earthquake Forces*, Detroit
- Ozcebe G, Saatcioglu M (1989) Hysteretic shear model for reinforced concrete members. *J. of Struct. Eng.* 115(1): 132-148
- Papia M, Russo G (1989) Compressive concrete strain at buckling of longitudinal reinforcement. *Journal of Struct. Eng.* 115(2): 382-397

- Park R, Paulay T (1975) Reinforced concrete structures. J. Wiley, New York
- Park YJ, Reinhorn AM, Kunnath SK (1987) Inelastic damage analysis of reinforced concrete frame-shear wall structures. Tech. Report NCEER 87-0008, State Univ. of New York at Buffalo
- Petrangeli M, Pinto P, Ciampi V (1999) Fiber element for cyclic bending and shear of R/C structures. I: Theory. J. of Eng. Mechanics 125(9): 994-1001
- Pincheira J, Dotiwala F, Souza J (1999) Seismic analysis of older reinforced Concrete columns. Earthquake Spectra 1999 15(2): 245-272
- Priestley MJN, Seible F, Calvi GM (1996) Seismic design and retrofit of bridges. J. Wiley, New York
- Priestley MJN, Verma R, Xiao Y (1994) Seismic shear strength of reinforced concrete columns. Journal of Structural Engineering 120(8): 2310-2329
- Ricles JM, Yang YS, Priestley MJN (1998) Modelling nonductile R/C columns for seismic analysis of bridges. J. of Struct. Eng. 124(4): 415-425
- Saatcioglu M, Ozcebe G (1989) Response of reinforced concrete columns to simulated seismic loading. ACI Struct. J. 86(1): 3-12
- Sezen H, Moehle JP (2004) Shear strength model for lightly reinforced concrete columns. J. of Struct. Eng. 130(11): 1692-1703
- Sivaselvan MV, Reinhorn AM (1999) Hysteretic models for cyclic behaviour of deteriorating inelastic structures. Technical Report MCEER-99-0018, University at Buffalo, State University of New York
- Takayanagi T, Derecho AT, Gorley WG (1979) Analysis of inelastic shear deformation effects in reinforced concrete structural wall systems. Proc. Nonlinear Design of Concrete Structures, CSCE-ASCE-ACI-CEB International Symposium, Univ. of Waterloo, Ontario, Canada
- Thom CV (1983) The Effects of inelastic shear on the seismic response of structures. PhD Thesis, University of Auckland, New Zealand
- Valles RE, Reinhorn AM, Kunnath SK, Li C, Madan A (1996) IDAR/C2D Version 4.0: A program for the inelastic damage analysis of buildings. Technical Report NCEER-96-0010, University at Buffalo, State University of New York
- Williams M, Villemure I, Sexsmith R (1997) Evaluation of seismic damage indices for concrete elements loaded in combined shear and flexure. ACI Struct. J. 94(3): 315-322

## FIGURE CAPTIONS

**Fig 1** Flexural sub-element

**Fig 2** Primary curve without degradation for shear force vs. shear deformation

**Fig 3** Shear-flexure interaction procedure

**Fig 4** Derivation of shear primary curve after modelling shear-flexure interaction effect: (a) Flexural primary curve in terms of member shear force and curvature ductility demand of the critical cross section; (b) shear ( $V - \gamma$ ) primary curve after modelling shear-flexure interaction

**Fig 5** Shear sub-element: (a) Prevailing gravity loading; (b) Prevailing seismic loading

**Fig 6** Variation of  $D_{tot}$  for the various combinations of  $D_{fl}$  and  $D_{sh}$

**Fig 7** Variation of  $D_{tot}$  with  $D_{max}$ , for  $D_{min}=0$  or  $D_{max}$

**Fig 8** Variation of  $D_{tot,min}$  with  $r_{max}$

**Fig 9** Variation of  $D_{tot,max}$  with  $r_{max}$

**Fig 10** Variation of  $D_{tot}$  with  $r_{max}$  for  $\xi=2/3$

**Fig 11** Variation of  $D_{tot}$  for the various combinations of  $\phi_{max}/\phi_u$  and  $\gamma_{max}/\gamma_u$

**Fig 12** Lehman et al. (1998) specimen 415: (a) Lateral load vs. total displacement; (b) Variation of  $D_{tot}$ ,  $D_{fl}$  and  $D_{sh}$  with the experimental load step; (c) Influence of the inelastic shear-flexure interaction effect on  $D_{sh}$  and  $D_{tot}$ ; (d) Comparison of the proposed index  $D_{tot}$  with the Park-Ang seismic damage index.

**Fig 13** Lynn et al. (1996) specimen 2CLH18: (a) Lateral load vs. total displacement; (b) Variation of  $D_{tot}$ ,  $D_{fl}$  and  $D_{sh}$  with the experimental load step; (c) Influence of the inelastic shear-flexure interaction effect on  $D_{sh}$  and  $D_{tot}$ ; (d) Comparison of the proposed index  $D_{tot}$  with the Park-Ang seismic damage index.

**Fig 14** Aboutaha et al. (1999) specimen SC9: (a) Lateral load vs. total displacement; (b) Lateral load vs. total displacement relationship, without modelling shear; (c) Variation of  $D_{tot}$ ,  $D_{fl}$  and  $D_{sh}$  with the experimental load step; (d) Comparison of the proposed index  $D_{tot}$  with the Park-Ang seismic damage index.

# FIGURES

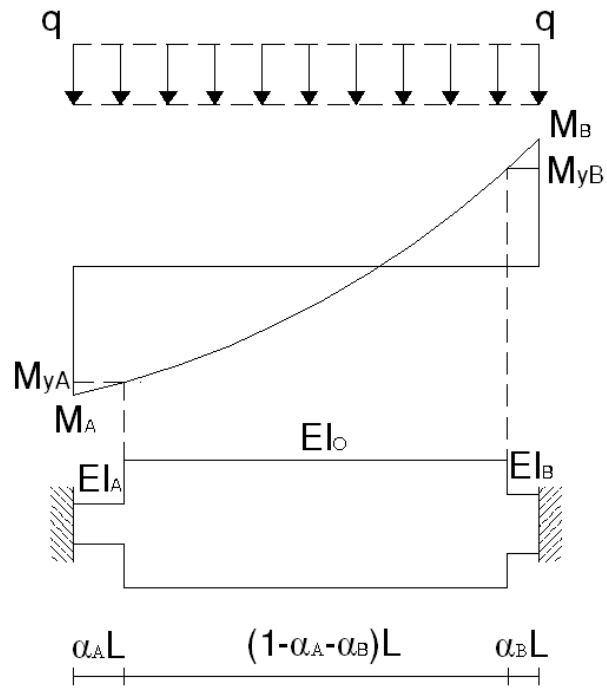


**Fig 1** Flexural sub-element

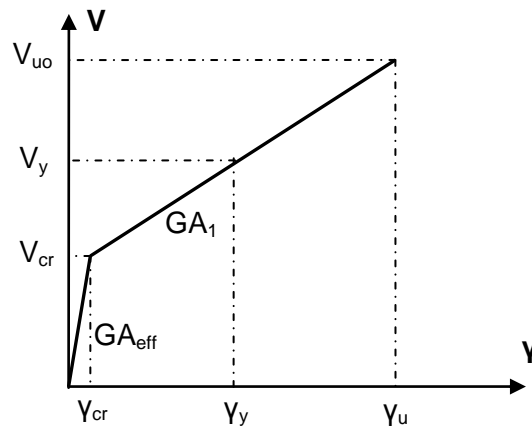


**Fig. 2** Primary curve without degradation for shear force vs. shear deformation

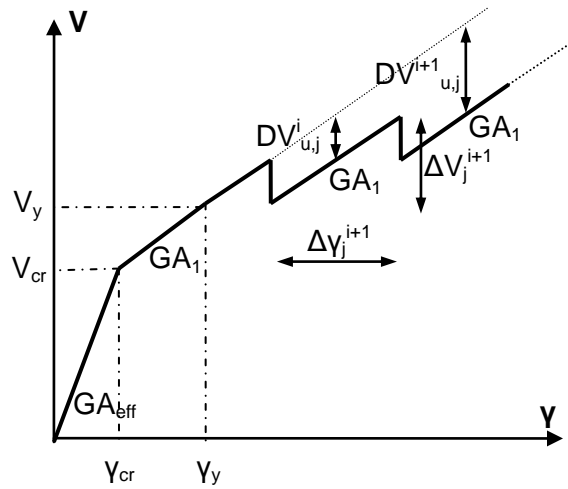


**Fig 3** Shear-flexure interaction procedure

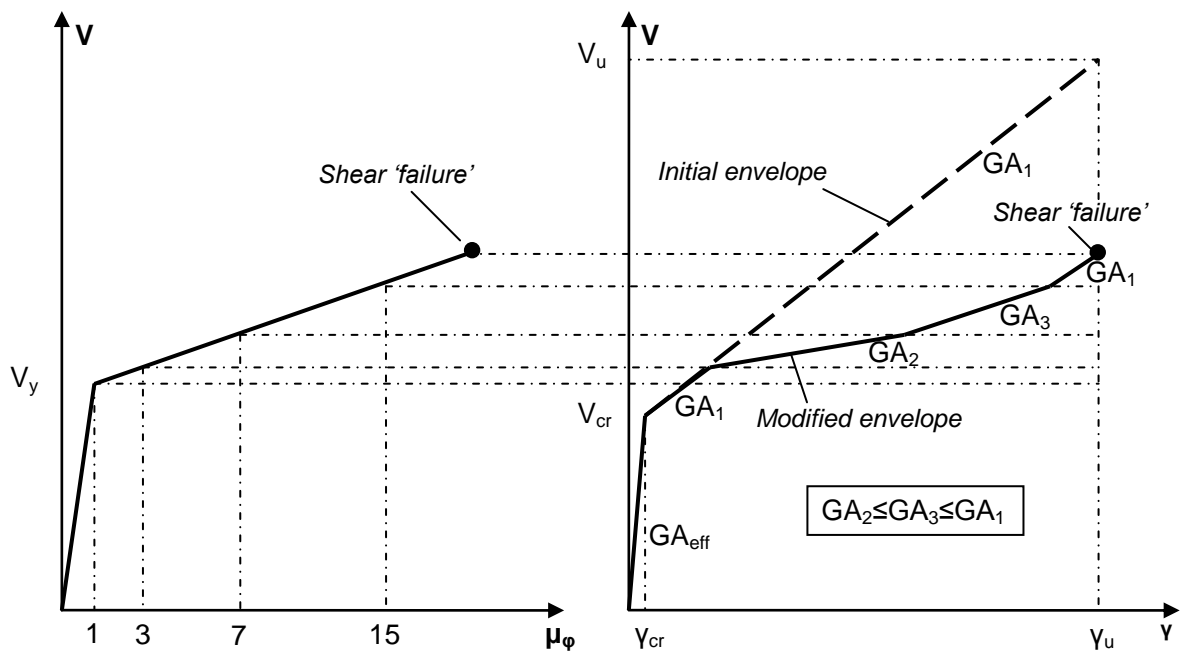


**Fig 4** Derivation of shear primary curve after modelling shear-flexure interaction effect: (a) Flexural primary curve in terms of member shear force and curvature ductility demand of the critical cross section; (b) shear ( $V - \gamma$ ) primary curve after modelling shear-flexure interaction

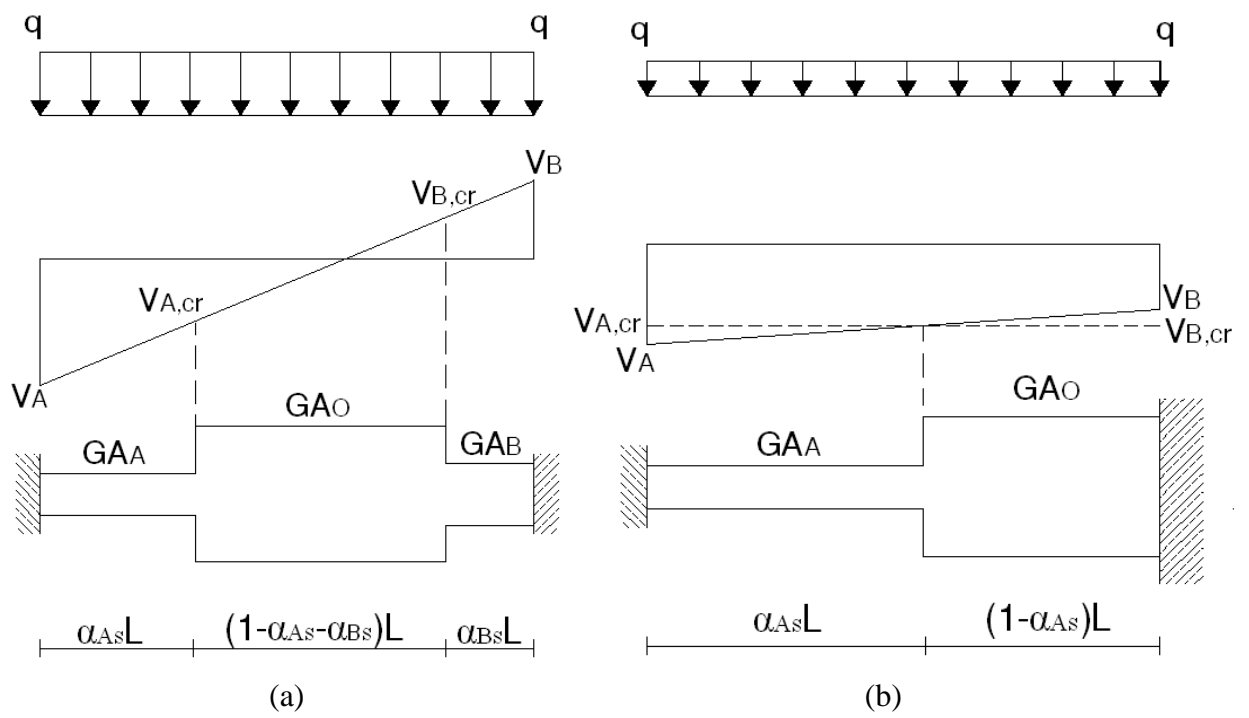


**Fig 5:** Shear sub-element: (a) Prevailing gravity loading; (b) Prevailing seismic loading

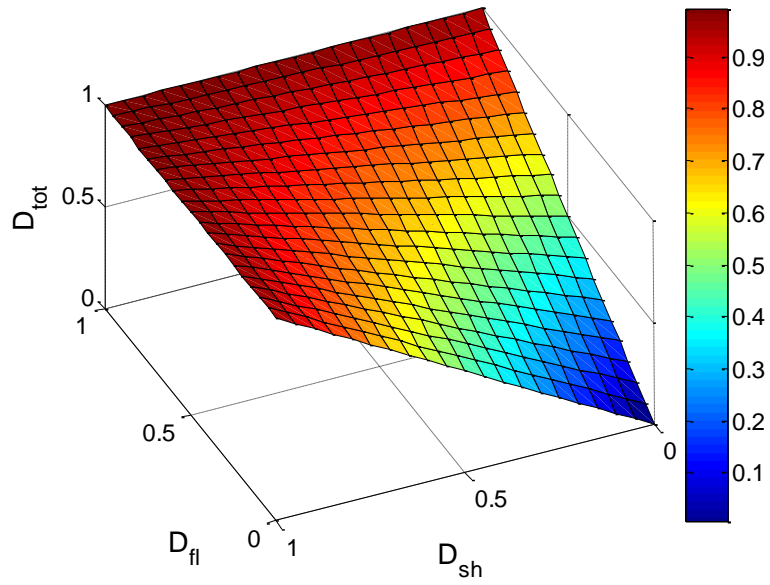


**Fig 6** Variation of  $D_{tot}$  for the various combinations of  $D_{fl}$  and  $D_{sh}$

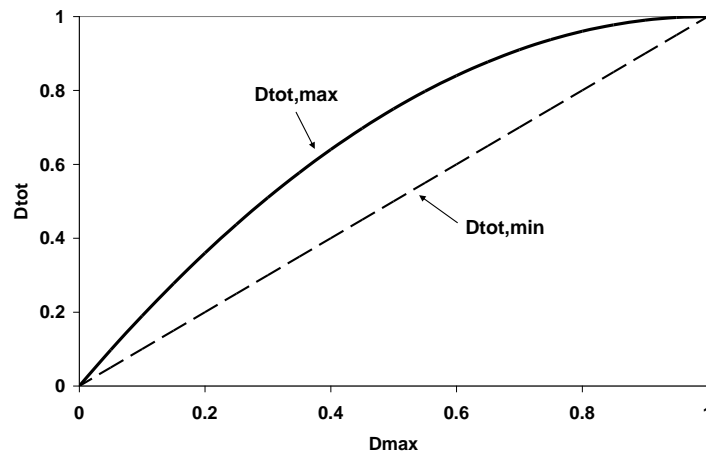


**Fig 7** Variation of  $D_{tot}$  with  $D_{max}$ , for  $D_{min}=0$  or  $D_{max}$

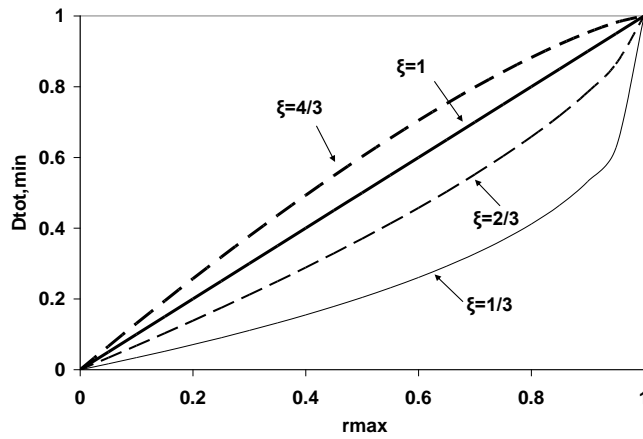


**Fig 8** Variation of  $D_{tot,min}$  with  $r_{max}$

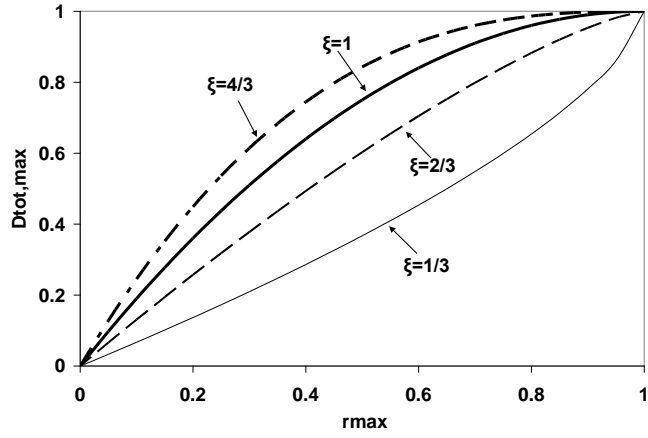


**Fig 9** Variation of  $D_{tot,max}$  with  $r_{max}$

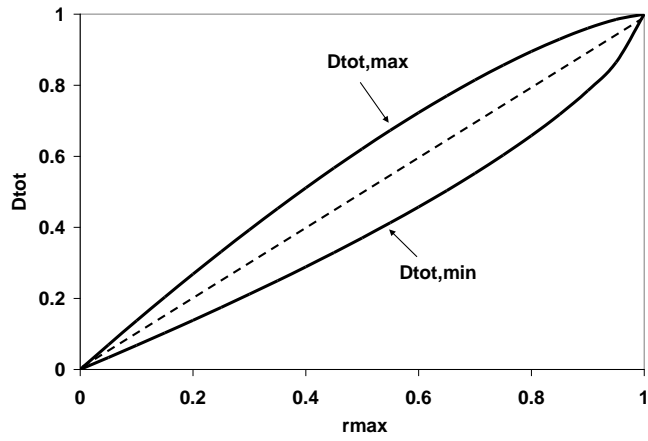


**Fig 10** Variation of  $D_{tot}$  with  $r_{max}$  for  $\xi=2/3$

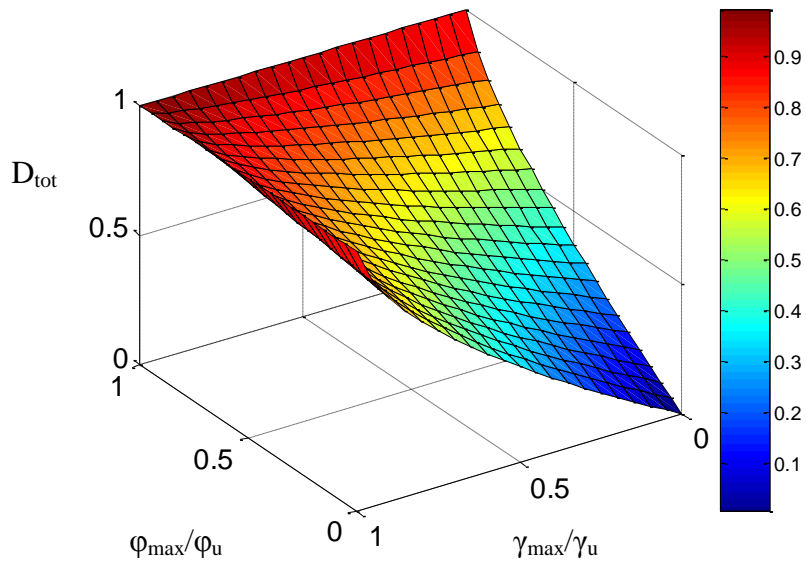


**Fig 11** Variation of  $D_{tot}$  for the various combinations of  $\phi_{max}/\phi_u$  and  $\gamma_{max}/\gamma_u$

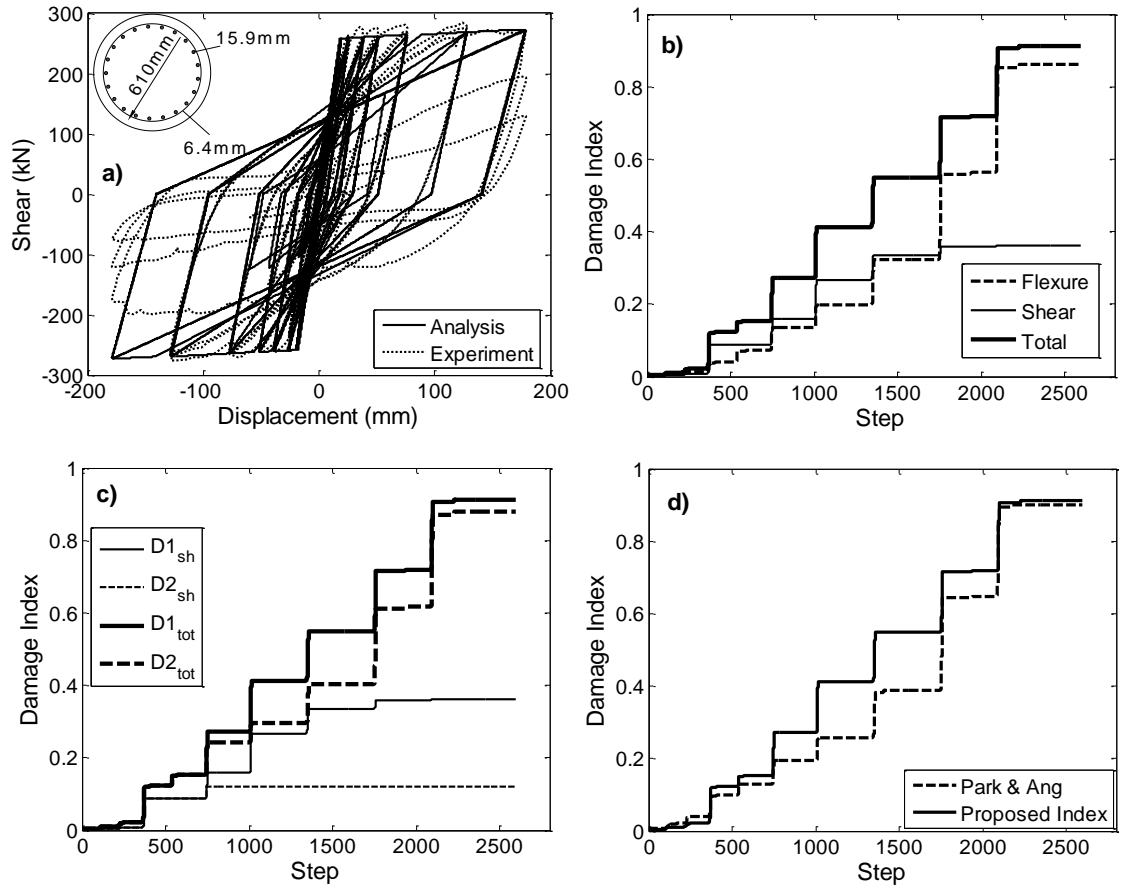


**Fig 12** Lehman et al. (1998) specimen 415: (a) Lateral load vs. total displacement; (b) Variation of  $D_{tot}$ ,  $D_{fl}$  and  $D_{sh}$  with the experimental load step; (c) Influence of the inelastic shear-flexure interaction effect on  $D_{sh}$  and  $D_{tot}$ ; (d) Comparison of the proposed index  $D_{tot}$  with the Park-Ang seismic damage index.

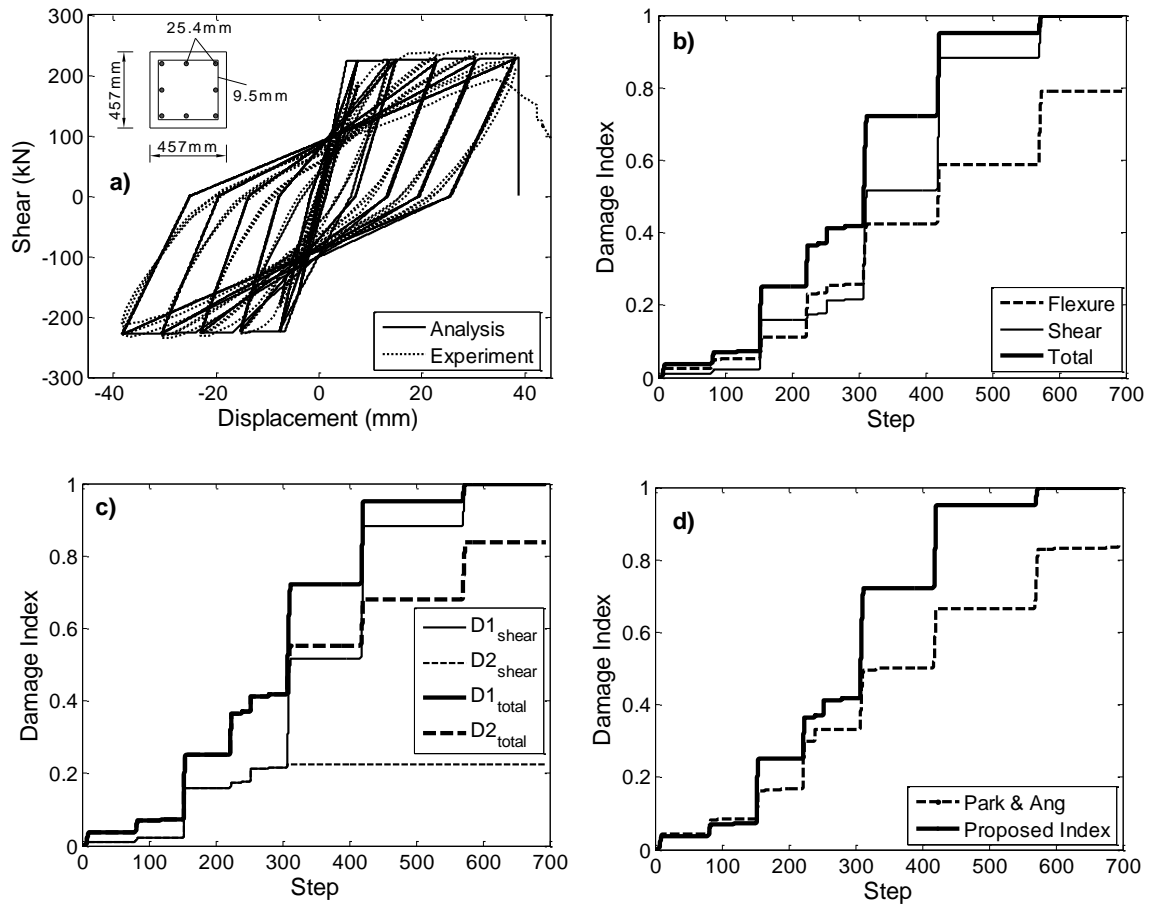


**Fig 13** Lynn et al. (1996) specimen 2CLH18: (a) Lateral load vs. total displacement; (b) Variation of  $D_{tot}$ ,  $D_{fi}$  and  $D_{sh}$  with the experimental load step; (c) Influence of the inelastic shear-flexure interaction effect on  $D_{sh}$  and  $D_{tot}$ ; (d) Comparison of the proposed index  $D_{tot}$  with the Park-Ang seismic damage index.

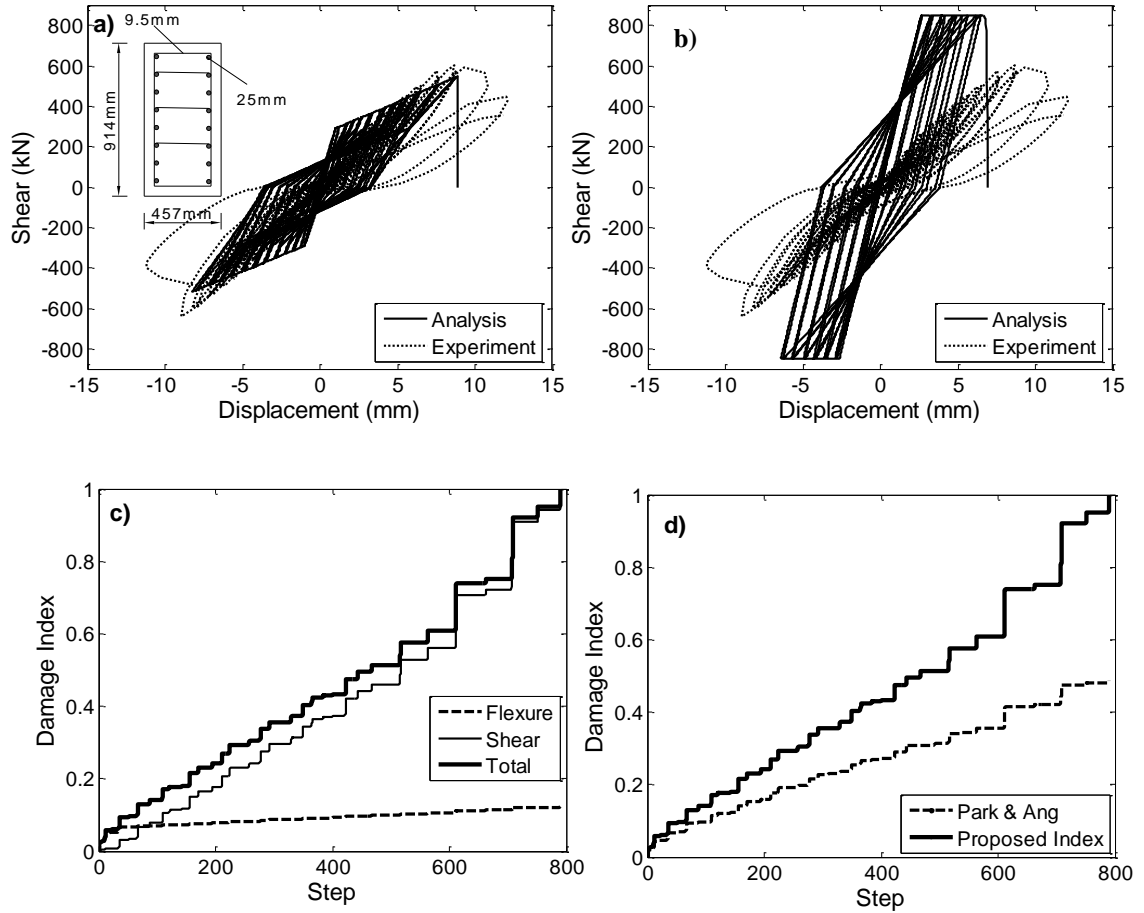


**Fig 14** Aboutaha et al. (1999) specimen SC9: (a) Lateral load vs. total displacement; (b) Lateral load vs. total displacement relationship, without modelling shear; (c) Variation of  $D_{tot}$ ,  $D_{fl}$  and  $D_{sh}$  with the experimental load step; (d) Comparison of the proposed index  $D_{tot}$  with the Park-Ang seismic damage index.